Structures of Calmodulin and a Functional Myosin Light Chain Kinase in the Activated Complex: A Neutron Scattering Study†

Joanna K. Krueger,‡ Glenn A. Olah,‡ Sue E. Rokop,‡ Gang Zhi,§ James T. Stull,§ and Jill Trewhella*,‡

Chemical Science and Technology Division, Mail Stop G758, Los Alamos National Laboratory, Los Alamos, New Mexico 87545, and Physiology Department, University of Texas Southwestern Medical Center, Dallas, Texas 75235-9040

Received February 5, 1997⊗

ABSTRACT: Calmodulin (CaM) is the major intracellular receptor for Ca^{2+} and is responsible for the Ca^{2+}-dependent regulation of a wide variety of cellular processes via interactions with a diverse array of target enzymes. Our current view of the structural basis for CaM enzyme activation is based on biophysical studies of CaM complexed with small peptides that model CaM-binding domains. A major concern with interpreting data from these structures in terms of target enzyme activation mechanisms is that the larger enzyme structure might be expected to impose constraints on CaM binding. Full understanding of the molecular mechanism for CaM-dependent enzyme activation requires additional structural information on the interaction of CaM with functional enzymes. We have utilized small-angle X-ray scattering and neutron scattering with contrast variation to obtain the first structural view of CaM complexed with a functional enzyme, an enzymatically active truncation mutant of skeletal muscle myosin light chain kinase (MLCK). Our data show that CaM undergoes an unhindered conformational collapse upon binding MLCK and activates the enzyme by inducing a significant movement of the kinase's CaM binding and autoinhibitory sequences away from the surface of the catalytic core.

Calmodulin (CaM) is the major intracellular receptor for Ca^{2+} and is responsible for the Ca^{2+}-dependent regulation of a diverse array of enzymes, including a number of kinases. The Ca^{2+}/calmodulin-dependent activation of myosin light chain kinase (MLCK) is one of the most studied examples of CaM−kinase interactions and has served as an important model. In its activated form MLCK catalyzes the transfer of the terminal phosphoryl group from a bound adenosine triphosphate moiety to the hydroxyl group of a serine located near the N-terminus of the myosin regulatory light chain. This phosphorylation event results in the potentiation of skeletal muscle contraction (Stull, 1988), plays important roles in nonmuscle events such as endothelial cell retraction, secretion, platelet aggregation, and exocytosis, and is essential for smooth muscle contraction (Stull *et al.*, 1996). Both skeletal and smooth/nonmuscle forms of MLCK contain a catalytic core homologous to that of other protein kinases, followed immediately by a carboxyl-terminal regulatory segment consisting of both an autoinhibitory sequence and a CaM-binding sequence (Kemp *et al.*, 1994; Stull *et al.*, 1995). The truncation mutant used in the studies reported here contains all of these elements [residues 257−607 of skeletal muscle MLCK (Gao *et al.*, 1995)]. The autoinhibition of MLCK has been the focus of many biochemical studies such as synthetic peptide inhibition analyses (Kemp *et al.*, 1987; Kemp & Pearson, 1990; Faux *et al.*, 1993), limited proteolysis (Walsh *et al.*, 1982; Ikebe *et al.*, 1987; Pearson *et al.*, 1988), and selected-site mutagenesis (Gallagher *et al.*, 1993; Krueger *et al.*, 1995) which have led to the conclusion that the regulatory segment of MLCK folds back on the catalytic core to inhibit kinase activity (Kemp & Pearson, 1991). Several interactions between specific acidic residues located along a distinct path on the surface of the catalytic core and specific basic residues within the regulatory segment (located up to 20 residues N-terminal to the calmodulin-binding sequence) have been implicated in maintaining inhibition. Mutation of these residues causes MLCK to become more easily activated by CaM but has no effect on substrate binding (Krueger *et al.*, 1995). The recent crystal structure of another related CaM-dependent protein kinase, CaM kinase I in its autoinhibited state, also demonstrates extensive interactions between its regulatory segment, including the CaM-binding sequence, and its catalytic core (Goldberg *et al.*, 1996).

CaM has an unusual dumbbell-shaped structure with two globular lobes connected by a single seven-turn, solvent-exposed α-helix (Babu *et al.*, 1985, 1988) that is flexible in solution (Heidorn & Trewhella, 1988; Barbato *et al.*, 1992). Each globular lobe contains two homologous helix−loop−helix structures that bind Ca^{2+}. Upon binding Ca^{2+}, calmodulin undergoes a number of structural changes including the exposure of a hydrophobic cleft in each globular lobe which interacts with hydrophobic residues from the target-enzyme binding sequence (Strynadka & James, 1988; Finn *et al.*, 1995; Kuboniwa *et al.*, 1995; Zhang *et al.*, 1995).

† This work was performed under the auspices of the DOE (Contract W-7410-ENG036) and supported by DOE Project KP-04-01-00-0 (J.T.) and NIH Grants GM40528 (J.T.), HL08874 (J.K.K.), and HL06296 (J.T.S.). Neutron scattering data were obtained using instrumentation supported by the NSF under Agreement DMR-9423101 at the Cold Neutron Research Facility at the National Institute of Standards Technology. X-ray scattering data were obtained at the Stanford Synchrotron Research Laboratory using instrumentation supported by the DOE (Basic Energy Sciences and Office of Health and Environmental Research) and the NIH Biomedical Resource Technology Program, Division of Research Resources.

* To whom correspondence should be addressed.

‡ Los Alamos National Laboratory.

§ University of Texas Southwestern Medical Center.

⊗ Abstract published in *Advance ACS Abstracts,* May 1, 1997.

S0006-2960(97)00270-5 CCC: $14.00

Small-angle X-ray and neutron scattering (Heidorn *et al.*, 1989), NMR (Ikura *et al.*, 1992), and X-ray crystallography (Meador *et al.*, 1992) studies of complexes of CaM with peptides based on CaM-binding sequences from smooth and skeletal muscle MLCKs demonstrate that CaM undergoes a conformational collapse that is achieved via the flexibility in the interconnecting helix region allowing the two lobes of CaM to come into close contact, encompassing the peptide. It has been proposed that formation of this compact structure is key to the release of the autoinhibitory mechanism. To directly test this proposal, we have completed small-angle X-ray and neutron scattering studies of the enzymatically active N-terminal truncation mutant of skeletal muscle MLCK with and without bound CaM. Small-angle scattering gives information on the overall shapes of proteins in solution. Because of the different neutron scattering properties of deuterium and hydrogen, deuterium labeling facilitates extraction of structural information on the individual components of the complex using neutron scattering with contrast variation. Thus the experiments described here provide the first structural view of CaM complexed with a functional enzyme.

MATERIALS AND METHODS

Protein Sample Preparation. MLCK (residues 257−607 of the skeletal muscle form) was purified as described by Gao *et al.* (1995) with the addition of a FPLC gel filtration (S12, Pharmacia) step. Column elution buffer contained 40 mM 3-(*N*-morpholino)propanesulfonic acid (MOPS), pH 8.0, 50 mM KCl, 10 mM magnesium acetate, 0.2 mM $CaCl_2$, 1 mM dithiothreitol (DTT), and 5% glycerol. Calmodulin, in both deuterated (dCaM) and nondeuterated (hCaM) forms, was prepared as described in Heidorn *et al.* (1989) with the addition of a FPLC S12 step using identical buffer conditions as used for the kinase. Samples of the complex were prepared with perdeuterated CaM (100dCaM) as well as partially deuterated CaM in which 50% of the nonexchangeable hydrogens were substituted with deuterium (50dCaM). Partial deuteration was achieved as described for troponin C (Olah *et al.*, 1994). The level of deuteration was determined using NMR by comparing total NMR intensity for hCaM versus dCaM from samples of known concentrations.

CaM·MLCK Complex Formation. Two independent sample preparations were used for neutron scattering experiments. All complexes were formed with Ca^{2+}-saturated CaM. For the first set of neutron experiments, samples of the complex were prepared with protein concentrations of 0.4−0.6 mg/mL with 1:1 100dCaM:MLCK in solutions containing 0%, 20%, and 40% D_2O and 1:1 50dCaM:MLCK in 0%, 80%, and 85% D_2O. For the second set of neutron experiments, more concentrated samples were used to give improved statistics in the scattering data: complexes were 1:1 100dCaM:MLCK with protein concentrations of 2.4 mg/mL in 0% D_2O and 1.8 mg/mL in 20% D_2O and 1:1 50dCaM:MLCK with protein concentrations of 0.6 mg/mL in 75% D_2O and 0.4 mg/mL in 85% D_2O. Furthermore, for the second set of neutron scattering experiments, glycerol-d_8 was used in the buffers to minimize contributions to the scattering from the hydrogen content of glycerol. Solvent density changes due to the presence of glycerol and/or glycerol-d_8 in the samples were taken into account in the data reduction and analysis. Samples for X-ray scattering experiments were prepared similarly to those for the neutron experiments.

Scattering Data Analysis. The scattering of neutrons (or X-rays) from a homogeneous solution of monodisperse particles (such as proteins or protein complexes) can be expressed as

$$I(Q) = |\int[\rho(\mathbf{r}) - \rho_s] \exp(-i\mathbf{Q}\cdot\mathbf{r})\, d\mathbf{r}|^2 \qquad (1)$$

where $Q = (4\pi \sin\theta)/\lambda$ is the amplitude of the scattering vector (2θ is the scattering angle and λ is the wavelength of the X-rays or neutrons), $\rho(\mathbf{r})$ and ρ_s are the scattering density for the protein and solvent, respectively, and the integration is taken over the volume of the particle. The scattering data were analyzed as previously described (Heidorn *et al*., 1989; Olah *et al*., 1994). In the case of neutrons one can take advantage of the large difference in neutron scattering lengths between hydrogen and deuterium, and by deuterating one component of a complex and using "contrast variation" (Ibel & Stuhrmann, 1975; Moore, 1981), one can obtain information on the conformations and dispositions of the individual components in the complex. Assuming internal scattering density fluctuations are negligible, the total scattering from a complex of a deuterated and nondeuterated protein can be written as

$$I(Q,\Delta\rho_C,\Delta\rho_K) = \Delta\rho_C{}^2 I_C(Q) + \Delta\rho_C\,\Delta\rho_K I_{CK}(Q) + \Delta\rho_K{}^2 I_K(Q) \qquad (2)$$

where the subscripts C and K refer to dCaM and MLCK, respectively. $\Delta\rho_C$ equals ρ_C - ρ_S, where ρ_C is the mean scattering density for dCaM. A similar definition holds for $\Delta\rho_K$. The three basic scattering functions in eq 2 are $I_C(Q)$ and $I_K(Q)$, representing the scattering due to the individual components in the complex, and $I_{CK}(Q)$ which is the cross term. The inverse Fourier transform of $I(Q)$ yields $P(r)$, the probable frequency distribution of interatomic vectors within the scattering particle. $P(r)$ goes to zero at the maximum linear dimension, d_{max}, of the scattering particle, and its zeroth and second moments give forward scatter, I_0, and radius of gyration, R_g, respectively.

Scattering Data Acquisition. X-ray scattering data were collected using beam line 4-2 at the Stanford Synchrotron Radiation Line (SSRL) (Wakatsuki *et al*., 1992), as well as the X-ray instrument at Los Alamos described in Heidorn and Trewhella (1988). X-ray data shown here are all from SSRL since the high-intensity synchrotron source gave dramatically increased statistical precision in the scattering data. Comparison of the synchrotron data with data measured on the same sample preparations at Los Alamos, using the much weaker sealed tube source, demonstrated any radiation damage effects because of the high X-ray intensities at the synchrotron were insignificant. All neutron scattering measurements were performed with the 30 m SANS instrument (NG3) at the National Institute of Standards and Technology (NIST) (Hammouda *et al.*, 1996) as described in Olah *et al.* (1994). Neutrons with a mean wavelength of 5.0 Å were used with a full width at half-maximum (FWHM) of 34% (unless noted otherwise). The first set of experiments utilized sample-to-detector distances of 1.3 m (λ = 5.5 Å/15% FWHM), 2.0 m, and 2.8 m and gave data in the Q-range 0.0275−0.17 $Å^{-1}$. The second experiment utilized sample-to-detector distances of 6 m and 1.5 m to give data

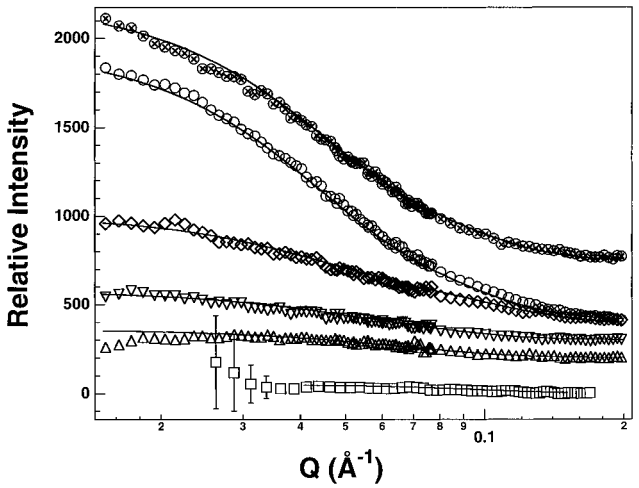

FIGURE 1: Scattering data for CaM·MLCK reduced to $I(Q)$ vs Q from X-ray scattering measurements (⊗) and neutron scattering measurements for samples in 0% (○), 20% (◇), 40% (□), 75% (△) and 85% (▽) D_2O. The scaling of the neutron scattering data reflects their relative contrast factors, while the X-ray scattering data are shown with an arbitrary scale relative to the neutron data for convenient presentation. Solid lines overlaying each data set represent $I(Q)$ vs Q calculated for a typical best two-ellipsoid fit to the data (see Figure 4).

over a broader Q-range 0.015−0.30 Å^{-1}. The excellent overlap of the 6 m and 1.5 m data in the Q-range 0.048−0.077 Å was used to scale these two data sets relative to each other. (This overlap is evident in Figure 1 noting that the 6 m data have a much smaller ΔQ than the 1.5 m data.) For both sets of neutron experiments sample cells were 1-mm path-length quartz cuvettes for 0%, 20%, and 40% D_2O, and 4-mm path-length quartz cuvettes for 75%, 80%, and 85% D_2O (since neutron transmissions were higher for these samples due to their lower H content).

Modeling the Scattering Data. The scattering data were modeled using a uniform density, two-ellipsoid model for the complex which implicitly ignores internal density fluctuations and assumes smooth ideal-shaped boundaries for the two protein components. Over the Q-range tested (0.015−0.15 Å^{-1}) these assumptions are reasonable. Best-fit one-ellipsoid models were initially determined for the CaM and MLCK components by calculating the associated scattering functions for randomly generated ellipsoids and comparing them to the basic scattering functions derived for the respective components using the scattering data from the complex. A Monte Carlo modeling routine was then written to generate ellipsoids with dimensions corresponding to the initial best fit values, but allowing them to vary randomly by 25−50% of the initial values (depending on the confidence with which each dimension was predicted by the initial fitting). Ellipsoid pairs were placed randomly in space such that their surfaces contacted and were allowed to overlap by up to 5 Å. This modeling approach has been used previously in our studies of the catalytic core of the cAMP-dependent protein kinase (Olah *et al.*, 1993), troponin C/troponin I (Olah & Trewhella, 1994), and calmodulin (Heidorn & Trewhella, 1988).

RESULTS AND DISCUSSION

Neutron scattering data from MLCK with bound deuterated CaM at five D_2O:H_2O ratios are shown in Figure 1. Only the data from the complex in 40% D_2O are shown from the first set of neutron exepriments. The neutron scattering data from samples of the complex in 0%, 20%, 75% and 85% D_2O show the wider Q-range measured in the second set of neutron experiments. X-ray scattering data from the complex are also shown in Figure 1. The X-ray data are binned to give similar Q-spacing and range as the second set of neutron scattering data.

Table 1: Structural Parameters of CaM·MLCK and Its Individual Components

	R_g (Å)	d_{max} (Å)	volume (Å^3)
X-ray scattering			
MLCK	27.2 ± 1.4	95 ± 10	57 000 ± 4 200
CaM·MLCK	34.0 ± 0.7	118 ± 4	79 200 ± 5 300
dCaM	20.7 ± 0.4	68 ± 3	21 800 ± 740
contrast series			
MLCK in the complex	24.6 ± 0.6	78 ± 4	49 750 ± 4 230
dCaM·MLCK	33.5 ± 1.0	100 ± 5	83 130 ± 9 870
dCaM in the complex	17.3 ± 0.4	49 ± 3	27 000 ± 3 750

Evaluation of Samples for Aggregation. Extraction of structural information on individual proteins or protein complexes in solution from scattering data requires samples that are rigorously aggregation free. The zero angle or forward scattering, I_0, is directly proportional to the molecular weight of the scattering particle and hence is extremely sensitive to aggregation (Kringbaum & Kugler, 1970). I_0 values derived from X-ray scattering data of MLCK and CaM·MLCK preparations were compared with those of a standard protein [lysozyme (Kringbaum & Kugler, 1970) or CaM (Heidorn & Trewhella, 1988)] known to be monodisperse, measured in the same sample cell on the same day. MLCK did not aggregate up to 3 weeks providing it was kept on ice in its standard buffer (see Materials and Methods). Addition of CaM to MLCK, however, always resulted in nonspecific aggregation of the complex within 24 h at 2 mg/mL protein concentrations, and within 48−72 h for less than 1 mg/mL protein concentrations. When perdeuterated CaM was used to form the complex, or when the complex was in solvents with >20% deuteration, the aggregation occurred more rapidly. The effects of aggregation were avoided by using 50% deuterated CaM for the samples in >50% D_2O buffers and by collecting all scattering data within a few hours of adding CaM to the kinase. All scattering data used for structural analysis were taken from samples that were determined to be aggregation free from an I_0 analysis. Molecular volumes, V, were also calculated from the small-angle X-ray scattering data and from the basic scattering functions derived from the neutron scattering data using the relationship $V = 2\pi^2 I_0/Q_i$ where Q_i is the scattering invariant (Porod, 1982). The volumes thus derived (Table 1) were all within experimental error of the values calculated using the protein's molecular weight and the specific volume for a typical protein of 0.72 cm^3/g, confirming that our samples were aggregation free for the duration of the scattering experiments. The rapid, nonspecific aggregation that we consistently observed for CaM·MLCK will likely make crystallization of this particular complex for high-resolution structural analysis difficult.

Extraction of the Basic Scattering Functions and P(r) Analysis. Each neutron scattering measurement at a given D_2O concentration gives an equation in the form of eq 2 ("contrast points"). An additional equation is obtained from the X-ray scattering data that has been appropriately scaled

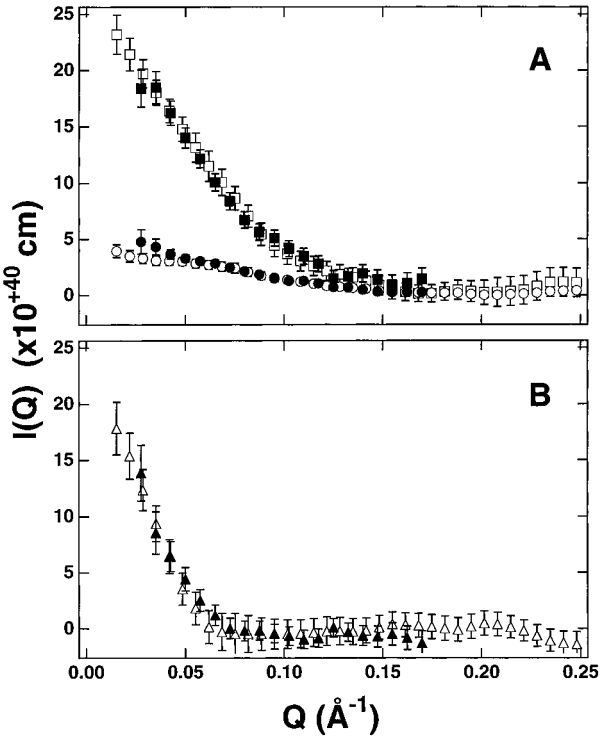

FIGURE 2: Basic scattering functions (A) $I_K(Q)$ (□), $I_C(Q)$ (○) and (B) $I_{CK}(Q)$ (Δ) vs Q, derived from the two neutron experiments (filled vs open symbols). The basic scattering functions derived from the two independent neutron experiments were in agreement and hence averaged for further analysis.

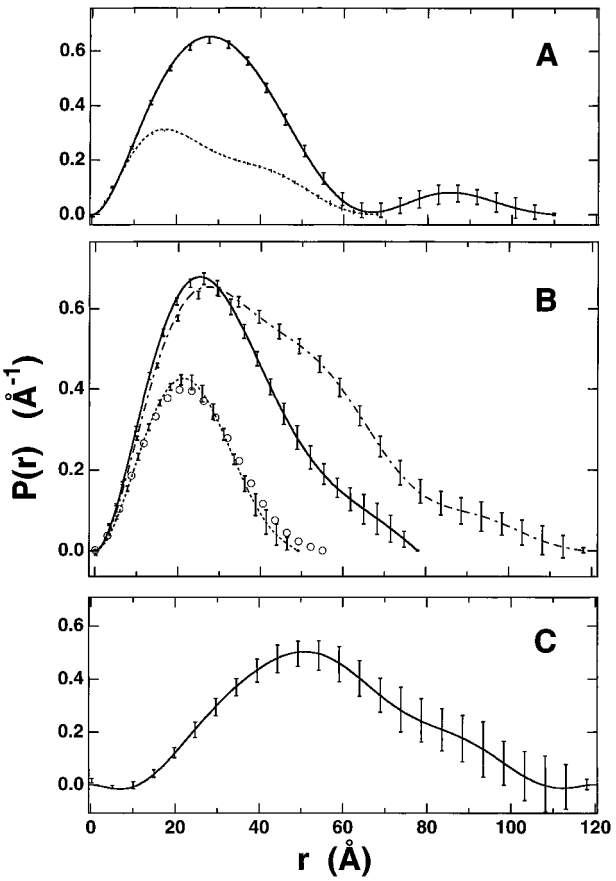

FIGURE 3: (A) $P(r)$ functions for dCaM (---) and MLCK (—) from X-ray scattering data obtained using the instruments at Los Alamos (Heidorn & Trewhella, 1988) and SSRL (Hammouda *et al.*, 1996). (B) $P(r)$ functions for dCaM (---) and MLCK (—) in the complex calculated using the basic scattering functions in Figure 2 and for CaM·MLCK (— · —) from X-ray scattering measurements. $P(r)$ calculated for the CaM portion only of the NMR solution structure of CaM·MLCK-I (○). (C) $P(r)$ calculated from the cross-term [$I_{CK}(Q)$]. $P(r)$'s were calculated using the method described by Moore (1980).

to the neutron scattering data (eq 24.8, Stuhrman, 1987). A multiple linear regression routine was written to solve the linear equations for the three basic scattering functions, $I_C(Q)$, $I_K(Q)$, and $I_{CK}(Q)$ (Figure 2). The corresponding $P(r)$ functions calculated as the inverse Fourier transform of $I(Q)$ vs Q (Moore, 1980) are given in Figure 3 along with the $P(r)$ functions calculated using X-ray scattering data from the CaM·MLCK complex, as well as its individual, uncomplexed components. The $P(r)$ function for free CaM calculated from the X-ray scattering data (Figure 3A) is characteristic of the bilobal CaM that has been previously observed (Heidorn & Trewhella, 1988; Seaton *et al.*, 1985). In contrast, the $P(r)$ function for CaM within the CaM·MLCK complex derived from the basic scattering function $I_C(Q)$ (Figure 3B) shows that the bound CaM has a compact, globular structure, which is reflected also by a decrease in R_g and d_{max} compared with free CaM (Table 1). These results are similar to those of our earlier neutron scattering studies (Heidorn *et al.*, 1989) of CaM complexed with MLCK-I, the 26-residue CaM-binding sequence from skeletal muscle MLCK (Blumenthal & Krebs, 1987). Further, the $P(r)$ for CaM in the complex is similar to the $P(r)$ calculated for the CaM portion only from the NMR structure of CaM·MLCK-I (Figure 3B). Thus, CaM undergoes a conformational collapse upon binding its sequence within the intact enzyme that is as dramatic as that observed for binding to MLCK-I.

$P(r)$ for unactivated MLCK calculated from the X-ray data (Figure 3A) shows a peak at ∼30 Å, consistent with a globular prolate ellipsoid shape with dimensions slightly larger than the catalytic core of the related cAMP-dependent protein kinase, cAPK (Olah *et al.*, 1993), and a tail extending to ∼95 Å. In comparing MLCK and cAPK, it should be remembered that the latter structure does not have the 32 N-terminal residues and 57 C-terminal regulatory and CaM-binding residues. The $P(r)$ function calculated from the basic scattering function of CaM-activated MLCK (Figure 3B) displays a more compact structure than the unactivated kinase. The "tail" observed for the unactivated MLCK is no longer present, and the peak shifts slightly to a lower r value (by ∼3 Å). R_g and d_{max} values are also smaller for the activated versus nonactivated MLCK by 2.6 and ∼17 Å, respectively (Table 1). Previously reported small-angle scattering measurements on cAPK detected reductions in R_g and d_{max} of 2 and 11 Å, respectively, upon the binding of its inhibitor peptide PKI(5−22)-amide (Olah *et al.*, 1993). This observed structural compaction was modeled as a closure of the cleft between the small and large lobes of cAPK via a simple rotation about a hinge defined by a pair of conserved glycine residues. The closed, PKI-bound cAPK structure also gave rise to a slight shift of 2−3 Å to smaller r in the position of the peak in its $P(r)$. The observed changes in the position of the peak in the $P(r)$ for MLCK upon CaM binding are of the same magnitude and direction as those observed for the closure of the cleft between the two lobes in the catalytic core of cAPK. Alternatively, the observed changes in MLCK upon complexation could arise from changes in the N-terminal and/or C-terminal sequence

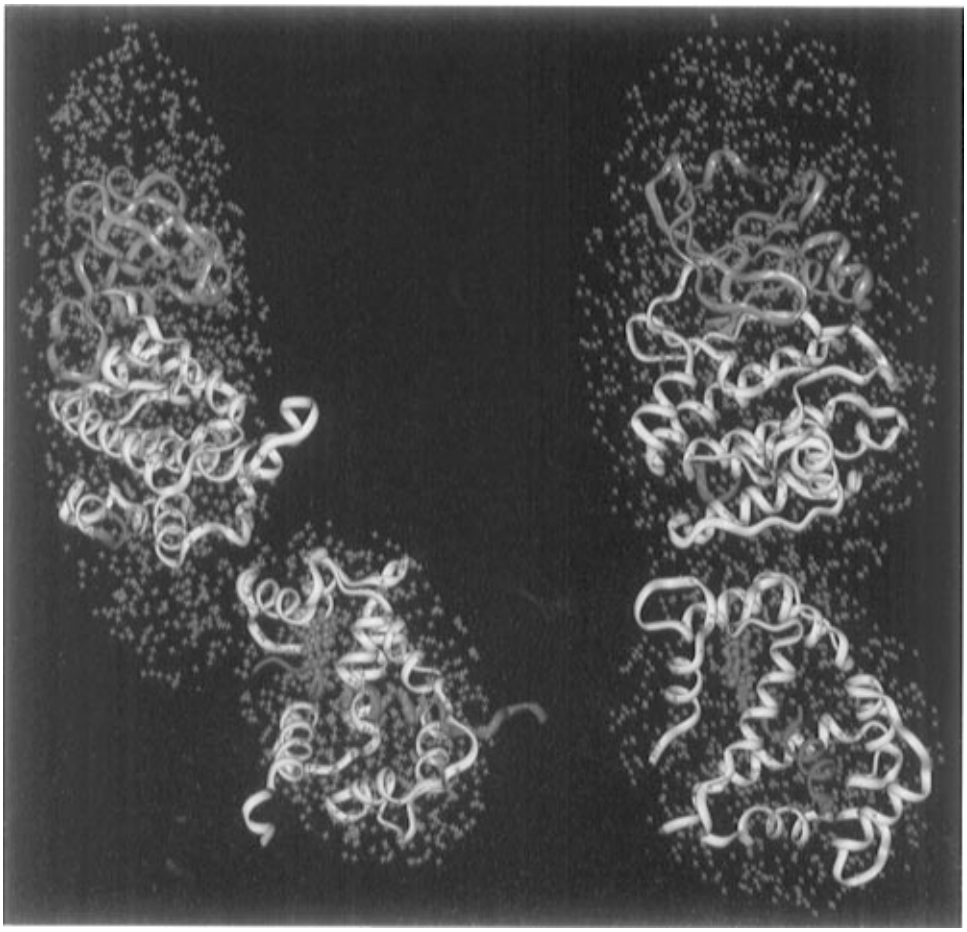

FIGURE 4: Two views rotated 90° about the long dimension of a typical best fit two-ellipsoid model for dCaM·MLCK. The green crosses represent the uniform density two-ellipsoid model. The conserved portion of the inhibited cAPK catalytic core (PDB no. 2cpk) residues 37−297, yellow and orange ribbons, is fit within the dimensions of the larger ellipsoid (*a*, *b*, and *c* equal 47.1, 25.1, and 17.0 Å). The N- and C-terminal residues of the catalytic core have been highlighted in red, and the small N-terminal lobe is in orange. This fit is only approximate as there are 32 and 57 residues N- and C-terminal, respectively, to the catalytic core whose structures are unknown. Further the orientation of the catalytic core is subject to the interpretation given in the text. The NMR structure (PDB no. 2bbm) of CaM, yellow ribbon, complexed with MLCK-I, red ribbon with ball-and-stick representation of the N-terminal Trp, is fit within the smaller ellipsoid (*a*, *b* and *c* equal 26.9, 22.6, and 16.6 Å).

segments induced by CaM binding. In either case, the activated MLCK is more compact than its unactivated form.

The $P(r)$ function for the CaM·MLCK complex calculated from X-ray data (Figure 3B) has a distinctive asymmetric shape. The peak (at ∼25 Å) and shoulder (at ∼55 Å) are indicative of a two-domain structure expected from the juxtaposition of the MLCK and CaM components. The inverse Fourier transform of $I_{CK}(Q)$ gives the probable distribution of interatomic vectors between the two components of the complex (Figure 3C), and the first moment of this transform gives the separation of the centers of mass of the two components, $D = 57$ Å.

Modeling the Scattering Data. Uniform density, two-ellipsoid models for the CaM·MLCK complex were used to aid in the interpretation of the scattering data. Of the 10^5 models generated, only 1750 fit the constraints of predicting the 0% D_2O neutron scattering data, specifically giving a $\chi^2 < 1.8$ and an R_g value within 2 Å of the measured value. Of these 1750 models, we found 100 best fit models evaluated by the more stringent criteria that the reduced $\chi^2 < 1.8$ for each X-ray and neutron scattering curve measured (see Figure 1). Each of the final 100 best fit models was very similar, having the same relative disposition of the smaller ellipsoid to the larger one and only minor differences (±2−4 Å) in the dimensions of the ellipsoids. The separation of the centers of mass for all the best fit models was consistently 55−60 Å, in excellent agreement with the values determined from the first moment of $I_{CK}(Q)$.

The two-ellipsoid model demonstrating the relative dispositions of MLCK and CaM within the activated complex is shown in Figure 4. CaM is seen to bind at a position distant from the equatorial plane perpendicular to the long axis of the ellipsoid representing the kinase. This result is really defined analytically by the combined constraints of the R_g and d_{max} values of the complex and its components, and the separation of their centers of mass. The primary contribution of the Monte Carlo calculations to the model is the determination of the axial dimensions of the two-ellipsoid shapes. The conserved portion of the catalytic core for all kinases based on the known crystal structure for inactive cAPK (Knighton *et al.*, 1991) and the NMR structure for CaM complexed with MLCK-I (Ikura *et al.*, 1992) were fit into their respective ellipsoids in our model. The two views shown of these fits demonstrate how well the asymmetric ellipsoids reflect the overall asymmetries in the molecular boundaries for both components. The MLCK component has 32 residues N-terminal and 57 residues C-terminal to the conserved catalytic core (defined as residues 37−297 of cAPK). The 32 N-terminal residues and 29 of the C-terminal residues that extend from the catalytic core to the beginning

of the CaM-binding sequence (residue 326) constitute ~13% of the total molecular mass (and hence volume) of the kinase. These residues would be expected to occupy the unfilled portions at the top and bottom of the kinase ellipsoid which constitute ~19% of its total volume. The small overlap between the kinase and CaM ellipsoids would reduce the unoccupied kinase volume by just a few percent. It seems noteworthy that the fit of the catalytic core in its ellipsoid leaves the G-helix, which sits packed against the activation loop, projecting out of the ellipsoid boundary. It is possible that, upon activation by CaM, the activation loop and hence the G-helix would undergo a structural change to bring it closer into the rest of the core. Similarly, there is a single CaM helix projecting out of its ellipsoid. This is the N-terminal helix, which is near the conserved Trp of the MLCK CaM-binding sequence that is believed to be key to CaM recognition. This N-terminal helix would therefore be expected to interact with the enzyme in the complex. It should be pointed out that the orientation of the catalytic core within the ellipsoid representing MLCK could be fit such that either the small N-terminal lobe or the large C-terminal lobe was closer to the CaM ellipsoid. If CaM were closer to the small lobe of MLCK, its binding sequence, and consequently the entire regulatory segment of the kinase, would be stretched across the longest dimension of the surface of the catalytic core, requiring approximately 20−25 residues to span at least 55 Å in a relatively extended conformation. In addition, the region of the kinase ellipsoid below the large C-terminal lobe would have to be somehow occupied by residues from the N-terminus. It seems more likely that CaM binds nearer to the large lobe, and the autoinhibitory sequence occupies the unfilled portion of the ellipsoid below the C-terminal lobe, leaving the N-terminal residues to account for the ellipsoid volume above the N-terminus. This view is represented in Figure 4.

Implications of the Scattering Results for the Activation Mechanism. Independent of whether CaM rests nearer the small or large lobe of MLCK in the activated complex, it is clear that it binds to a site that is away from the catalytic cleft. In addition, a substantial movement of the MLCK CaM-binding sequence away from the catalytic core is required in order for CaM to achieve the observed unhindered conformational collapse. This movement must involve all of the CaM-binding residues, in addition to residues immediately N- and C-terminal to that sequence, i.e., including at least part of the autoinhibitory sequence. The crystal structure of a related CaM-dependent kinase, CaM kinase I (Goldberg *et al.*, 1996), in its autoinhibited state shows that the CaM-binding sequence in CaM kinase I sits with its N-terminal residues near the hinge at the back side of the catalytic cleft and extends to make contacts with the small ATP-binding lobe. The CaM Kinase I and the non-CaM activated twitchin kinase (Hu *et al.*, 1994) autoinhibitory sequences both form extensive contacts along a distinct path on the larger C-terminal lobe. Our earlier mutagenesis studies also indicate that there is an extensive network of contacts between the large C-terminal lobe of MLCK and its autoinhibitory region (Gallagher *et al.*, 1993; Krueger *et al*., 1995). CaM binding away from the catalytic cleft requires a significant portion of this network of contacts to be disrupted, inferring substantial movement of the autoinhibitory sequence upon CaM binding. The autoinhibitory sequence may be quite flexible once removed from specific interactions with the core, and since small-angle scattering data give information only on the time and ensemble average of the solution structure, location of the bound CaM with respect to the kinase may vary about an average position. Assuming further structural homology between CaM kinase I and MLCK, movement of the CaM-binding sequence would also remove constraints on the relative rotations of the two lobes of the catalytic core, which could give rise to changes in the relative dispositions of the small and large domains of the catalytic core.

Our data thus support a picture of the molecular mechanism of CaM activation in which CaM collapses about its binding sequence within the regulatory segment of MLCK and in doing so causes part or all of the autoinhibitory sequence to be removed from its binding site on the surface of the unactivated catalytic core, thus facilitating substrate access to the catalytic site. Higher resolution data are needed to completely define the chemical contacts that are formed and broken in this process. Importantly, we have shown here that the mechanism proposed for CaM-mediated release of autoinhibition based on biochemical data and studies of CaM−peptide complexes is reflected in the conformational changes and interactions observed for a functionally intact CaM−kinase complex.

ACKNOWLEDGMENT

We thank Nicholas A. Bishop for technical assistance in the neutron data acquisition and reduction and Deanna Kergil for technical contributions to preparation of samples for preliminary scattering experiments. We thank Griselda Hernández for the NMR data used to calculate the deuteration levels in calmodulin. We also thank Drs. Susan Krueger and Charles Glinka for assistance in the neutron scattering data acquisition at NIST and Dr. H. Tsurata for assistance in X-ray scattering data acquisition at SSRL. We acknowledge the support of the National Institute of Standards and Technology, U.S. Department of Commerce, in providing neutron research facilities used in this work.

REFERENCES

Babu, Y. S., Sack, J. S., Greenhough, T. J., Bugg, C. E., Means, A. R., & Cook, W. J. (1985) *Nature 315*, 37.
Babu, Y. S., Bugg, C. E., & Cook, W. J. (1988) *J. Mol. Biol. 204*, 191.
Barbato, G., Ikura, M., Kay, L. E., Pastor, R. W., & Bax, A. (1992) *Biochemistry 31*, 5269.
Blumenthal, D. K., & Krebs, E. G. (1987) *Methods Enzymol. 139*, 191.
Faux, M. C., Mitchelhill, K. I., Katsis, F., Wettenhall, R. E. H., & Kemp, B. E. (1993) *Mol. Cell. Biochem. 128*, 81.
Finn, B. E., Evenäs, J., Drakenberg, T., Waltho, J. P., Thulin, E., & Forsén, S. (1995) *Nat. Struct. Biol. 2*, 777.
Gallagher, P. J., Herring, B. P., Trafny, A., Sowadski, J., & Stull, J. T. (1993) *J. Biol. Chem. 268*, 26578.
Gao, Z.-H., Zhi, G., Herring, B. P., Moomaw, C., Deogny, L., Slaughter, C. A., & Stull, J. T. (1995) *J. Biol. Chem. 271*, 1025.
Goldberg, J., Nairn, A. C., & Kuriyan, J. (1996) *Cell 84*, 875.
Hammouda, B., Barker, J. G., & Krueger, S. (1996) *Small-Angle Neutron Scattering Manuals* (NIST), Gaithersburg, MD.
Heidorn, D. B., & Trewhella, J. (1988) *Biochemistry 27*, 909.
Heidorn, D. B., Seeger, P. A., Rokop, S. E., Blumenthal, D. K., Means, A. R., Crespi, H., & Trewhella, J. (1989) *Biochemistry 28*, 6757.
Hu, S.-H., Parker, M. W., Lei, J. Y., Wilce, M. C. J., Benian, G. M., & Kemp, B. E. (1994) *Nature 369*, 581.
Ibel, K., & Stuhrmann, H. B. (1975) *J. Mol. Biol. 93*, 255.

Ikebe, M., Stepinska, M., Kemp, B. E., Means, A. R., & Hartshorne D. J. (1987) *J. Biol. Chem. 262*, 13828.
Ikura, M., Clore, G. M., Gronenborn, A. M., Zhu, G., Klee, C. B., & Bax, A. (1992) *Science 256*, 632.
Kemp, B. E., & Pearson, R. B. (1990) *Trends Biochem. Sci. 15*, 342−346.
Kemp, B. E., & Pearson, R. B. (1991) *Biochim. Biophys. Acta 1094*, 67.
Kemp, B. E., Pearson, R. B., Guerriero, V., Jr., Bagchi, I., & Means, A. R. (1987) *J. Biol. Chem. 262*, 2542.
Kemp, B. E., Parker, M. W., Hu, S., Tiganis, T., & House, C. (1994) *Trends Biochem. Sci. 19*, 440.
Knighton, D. R., Zheng, J. H., Ten Eyck, L. F., Ashford, V. A., Xuong, N. H., Taylor, S S., & Sowadski J. M. (1991) *Science 253*, 407.
Kringbaum, W. R., & Kugler, F. R. (1970) *Biochemistry 9*, 1216.
Krueger, J. K., Padre, R. C., & Stull, J. T. (1995) *J. Biol. Chem. 270*, 16848.
Kuboniwa, H., Tjandra, N., Grzesiek, S., Ren, H., Klee, C. B., & Bax, A. (1995) *Nat. Struct. Biol. 2*, 768.
Meador, W. E., Means, A. R., & Quiocho, F. A. (1992) *Science 257*, 1251.
Moore, P. B. (1980) *J. Appl. Crystallogr. 13*, 168.
Moore, P. B. (1981) *J. Appl. Crystallogr. 14*, 237.
Olah, G. A., & Trewhella, J. (1994) *Biochemistry 33*, 12800.
Olah, G. A., Mitchell, R. D., Sosnick, T. R., Walsh, D. A., & Trewhella, J. (1993) *Biochemistry 32*, 3649.
Olah, G. A., Rokop, S. E., Wang, A. C.-L., Blechner, S. L., & Trewhella, J. (1994) *Biochemistry 33*, 8233.
Pearson, R. B., Wettenhall, R. E. H., Means, A. R., Hartshorne, D. J., & Kemp, B. E. (1988) *Science 241*, 970.
Porod, G. (1982) in *Small Angle X-ray Scattering*, pp 17−51, Academic Press, New York.
Seaton, B. A., Head, J. F., Engelman, D. M., & Richards, F. M (1985) *Biochemistry 24*, 6740.
Strynadka, N. C. J., & James, M. N. G. (1988) *Proteins: Struct., Funct., Genet. 3*, 17.
Stuhrman, H. B. (1987) in *Methods of Experimental Physics*, pp 367−403, Academic Press, Inc., New York.
Stull, J. T. (1988) in *Molecular Aspects of Cellular Regulation* (Cohen, P., & Klee, B. C., Eds.) Vol. 5, pp 91−119, Elsevier, Amsterdam.
Stull, J. T., Krueger, J. K., Zhi, G., & Gao, Z.-H. (1995) in International Symposium on Regulation of the Contractile Cycle in Smooth Muscle, Mie, Japan.
Stull, J. T., Krueger, J. K., Kamm, K. E., Gao, Z.-H., Zhi, G., & Padre, R. (1996) in *Biochemistry of Smooth Muscle Contraction* (Barany, M., Ed.) pp 119−128, Academic Press, Inc., San Diego.
Wakatsuki, S., Hodgson, K. O., Eliezer, D., & Rice, M. (1992) *Rev. Sci. Instrum. 63*, 1736.
Walsh, M. P., Dabrowska, R., Hinkins, S., & Hartshorne, D. J. (1982) *Biochemistry 21*, 1919.
Zhang, M., Tanaka, T., & Ikura, M. (1995) *Nat. Struct. Biol. 2*, 758.

BI9702703